

Chemical Science

Accepted Manuscript



This is an *Accepted Manuscript*, which has been through the Royal Society of Chemistry peer review process and has been accepted for publication.

Accepted Manuscripts are published online shortly after acceptance, before technical editing, formatting and proof reading. Using this free service, authors can make their results available to the community, in citable form, before we publish the edited article. We will replace this *Accepted Manuscript* with the edited and formatted *Advance Article* as soon as it is available.

You can find more information about *Accepted Manuscripts* in the [Information for Authors](#).

Please note that technical editing may introduce minor changes to the text and/or graphics, which may alter content. The journal's standard [Terms & Conditions](#) and the [Ethical guidelines](#) still apply. In no event shall the Royal Society of Chemistry be held responsible for any errors or omissions in this *Accepted Manuscript* or any consequences arising from the use of any information it contains.



www.rsc.org/chemicalscience



Journal Name

ARTICLE

CH₃NH₃PbI₃ Perovskite Single Crystals: Surface Photophysics and its Interaction with the Environment

G. Grancini,^{a, *, †} V. D'Innocenzo,^{a, b} E. R. Dohner,^c N. Martino,^{a, b} A. Ram Srimath Kandada,^a E. Mosconi,^d F. De Angelis,^d H. I. Karunadasa,^c E.T. Hoke,^e and A. Petrozza^{a, *}

Received 00th January 20xx,
Accepted 00th January 20xx

DOI: 10.1039/x0xx00000x

www.rsc.org/

Here we identify a structural inhomogeneity on a micrometer scale across the surface of a CH₃NH₃PbI₃ perovskite single crystal. At the crystal edge a local distortion of the crystal lattice is responsible for a widening of the optical bandgap and a faster photo-carrier recombination. These effects are inherently present at the edge of the crystal, and further enhanced upon water intercalation, as a preliminary step in the hydration of the perovskite material.

Introduction

Hybrid perovskite based solar cells have already exceeded 20.1% certified power conversion efficiencies.¹⁻² However, a clear understanding of the relationship between the optoelectronic properties of these materials and their morphology is lacking due to the large degree of structural variability within samples. Hybrid perovskites are usually deposited as polycrystalline thin-films with variable mesoscale morphology.³⁻⁵ Depending on the growth conditions, the obtained grain size typically ranges from tens to thousands of nm.³⁻⁵ To overcome this issue, perovskite single crystals are the ideal sample for understanding the inherent properties of the material, providing insight into their full potential once embodied in optoelectronic devices. Several recent studies have reported conflicting optical properties for MAPbI₃ (MA = CH₃NH₃⁺) single crystals.⁶⁻⁹

Here we provide a unifying picture, by highlighting the variation of the structural and optical properties across the crystal surface at a micrometer scale and by elucidating its interaction with the environment. Indeed, the optical properties we reveal at the crystal edges more closely resemble those of polycrystalline MAPbI₃ thin films used in optoelectronic devices.^{11, 18} These local probes of the structure

and photophysical dynamics of the single crystal edge sites provide a systematic method for studying and optimizing the active interfaces, of high technological impact in polycrystalline perovskite films.

Results and discussion

Figure 1a-c shows the SEM image of the single crystal and higher resolution images of the region investigated. Specifically, we probe points at the centre of the crystal face (point A) or at the crystal edge (point B). The local photoluminescence spectra and dynamics have been measured with a spatial resolution of ~1 μm (micro-PL here after, see Experimental section for details) with the aim to probe the optical properties of the single crystal surface at a local scale. Example PL spectra and decay dynamics from the centre of the crystal face and the edge (taken at points A and B, respectively) are presented in Figure 1d, e. The PL spectrum blue-shifts and the PL decay accelerates when moving from the centre to the crystal edge. In particular, the higher-energy PL from the crystal edge (Figure 1c, point B) consists mainly of a fast component (~40 ns, see Figure 1e), along with a minor contribution from a long-lived tail (~600 ns). On the contrary, for the lower-energy PL from the crystal centre (Figure 1c, point A) the long-lived component dominates over the fast decay. Though the actual shift cannot be accurately quantified due to re-absorption effects that cannot be fully disregarded, together, these observations suggest that the spatial variation of the PL spectra arises from energetic inhomogeneity across the crystal. Such a conclusion can be further corroborated by looking at the spatial variation of the transient reflectance (TR) signal across the crystal face, which probes the semiconductor band edge (by monitoring the band edge photobleaching upon carrier cooling -see Fig. S1 in the SI with relative discussion-).

^a Center for Nano Science and Technology @Polimi, Istituto Italiano di Tecnologia, via Giovanni Pascoli 70/3, 20133, Milan, Italy

^b Dipartimento di Fisica, Politecnico di Milano, Piazza L. da Vinci, 32, 20133 Milano, Italy

^c Department of Chemistry, Stanford University, 337 Campus Drive, Stanford, California 94305, USA

^d Computational Laboratory for Hybrid/Organic Photovoltaics (CLHYO), CNR-ISTM, I-06123, Perugia, Italy

^e Department of Materials Science and Engineering, Stanford University, 476 Lomita Mall, Stanford, California 94305, USA

[†] present address: EPFL Valais Wallis, Rue de l'Industrie 17, CH-1951 Sion (Switzerland)

Electronic Supplementary Information (ESI) available: See DOI: 10.1039/x0xx00000x

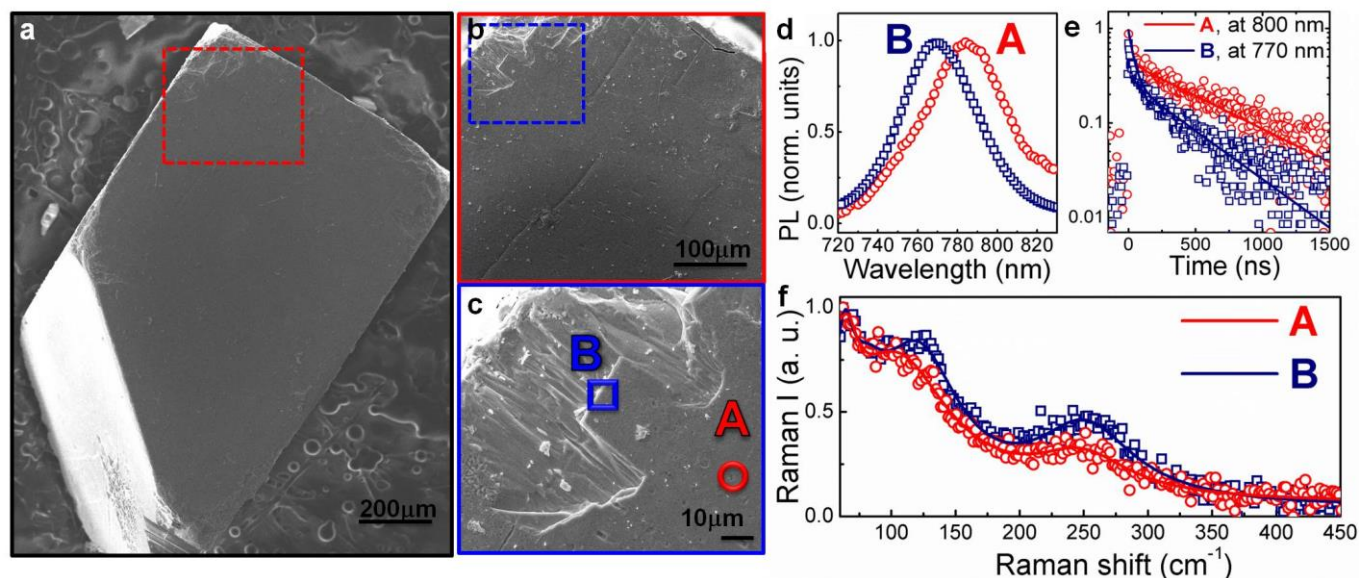


Figure 1. (a) Top view SEM image of a mm-large MAPbI₃ single crystal (see Figure S2 for XRD data); (b) Enlarged view of the SEM in the top-left area of (a); (c) higher-resolution image of the SEM in the top-left area of (b) where spot A (towards the centre of the crystal face) and B (at the edge of the crystal face) have been measured, respectively; (d) PL spectra on spot A and B upon excitation at 690nm (fluence $\sim 10 \mu\text{J}/\text{cm}^2$) under N₂ atmosphere (e) PL time decays at 770nm (peak of point B PL spectrum) and 800nm (peak of point A PL spectrum), solid lines represent the fits ($y=0.5 \exp(-t/\tau_1)+0.2 \exp(-t/\tau_2)$, $\tau_1=630\text{ns}$, $\tau_2=40\text{ns}$ fits the decay at 800nm; $y=0.2 \exp(-t/\tau_1)+0.44 \exp(-t/\tau_2)$, $\tau_1=500\text{ns}$, $\tau_2=38\text{ns}$ fits the decay at 770nm). (f) Raman spectra from point B (blue squares) and point A (red dots) along with fitting results (solid lines). The measurement has been done under N₂ atmosphere.

Considering that the excitation wavelength of 690nm has an absorption depth of approximately 250nm,¹⁰ surface effects (e.g., dangling bonds, under-coordinated atoms) will dominate the micro-PL measurement, certainly significant when probing the surface edges. We suggest that these edge surface effects are responsible for the blue-shifted, faster decaying component of the PL. In polycrystalline perovskite thin films it has been demonstrated¹⁰⁻¹² that deformation of the inorganic cage through interactions with the organic cations can compress the lattice, resulting in an increased bandgap.¹⁰⁻¹⁵ Specific vibrational modes have been assigned as evidence for these lattice structural distortions.^{11, 16, 17}

To better understand the origin of the spatially inhomogeneous PL, we measured the micro-Raman spectra at a $\sim 1\mu\text{m}$ scale resolution on exactly the same points on which the micro-PL spectra were measured (Figure 1f; see Experimental section for details on the set-up). Excitation at the centre (point A) and the edge (point B) of the crystal face leads to different spectra, suggesting a restructuring of the crystal surface at the edges. The former shows a peak at 109cm^{-1} , assigned to the Pb-I stretching mode¹⁷ and a broad band at 250cm^{-1} , previously assigned to the torsional mode of the MA cation.^{11, 17} When moving to the edge, we observe that the frequency of the Pb-I stretching mode is blue-shifted (towards 120cm^{-1}) and the peak gains intensity, while the band at 250cm^{-1} slightly shifts and gets more intense. A similar trend has been previously observed for MAPbI₃ nanocrystals grown within a mesoporous oxide scaffold, which were reported to be more distorted with respect to micrometer-size MAPbI₃ crystallites deposited on a flat glass substrate.¹⁶ This result

suggests that lattice strain at the crystal edges can be responsible for the blue-shifted PL. The above observations indicate that the edges of the MAPbI₃ single crystal differ optically, energetically and structurally from the centre of the crystal face. This is not surprising, considering that defects and lattice reconstructions are common at crystal edges. Note also that the micro-PL spectra we measure at the crystal edges, rather than crystal centre PL, more closely resemble the usual PL spectra observed for MAPbI₃ polycrystalline thin films.^{11, 18, 19} Thus, we believe that the distorted crystal surface provides a model for the properties of polycrystalline thin films with small grains where surface effects at high defect densities, grain boundaries and active interfaces dominate and dramatically impact the device operation.

Because the surface is exposed to the surrounding atmosphere, we investigated how the optical properties of the single crystal surface are sensitive to environmental interaction, in particular to the presence of moisture. The interaction between MAPbI₃ and water is of particular concern as moisture has been shown to dramatically impact not only the perovskite film growth and crystallization dynamics²⁰⁻²⁵ but also accelerate material degradation.²⁵⁻²⁸ Figure 2 shows the macro-PL spectra measured on the whole crystal surface in (a) vacuum, (b) under low humidity (dry air with water content $<10 \text{ ppm/mol}$) and (c) high humidity (ambient conditions, $\sim 50\%$ relative humidity) (see Figure S3 for a cartoon of the excitation-collection geometry).

Here we are probing the signal from the whole crystal surface, including the edges. As shown below, in vacuum (Figure 2a), the PL spectrum appears broad and asymmetric. Upon

increasing exposure to humidity, the blue component becomes dominant (Figure 2b, c) resulting in a sharp spectrum (FWHM ~ 22 nm) peaking at 770nm and the PL decay dynamics are shortened (Figure 2d, e) showing a complete quenching of the longer-wavelength emission at ambient humidity. The PL spectra were taken within a few minutes of changing the test chamber atmosphere, indicating that the spectral changes are rapid. Such behaviour indicates that in ambient conditions, the reconstruction of the crystal surface induced by lattice distortion becomes more significant.

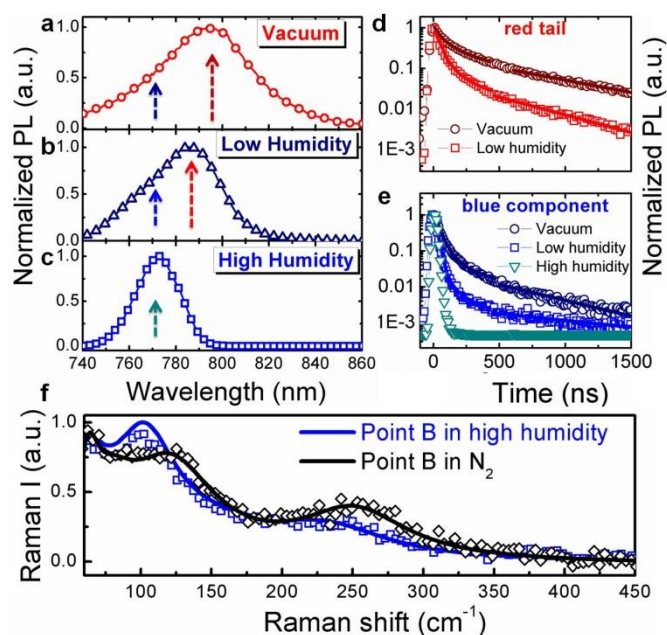


Figure 2. Normalized PL spectra (a-c) and dynamics (d, e, respectively) at the wavelength indicated by the arrows in Figure 2a-c, collected in vacuum (a), in low humidity atmosphere (b) and high humidity (c); fluence $\sim 10 \mu\text{J}/\text{cm}^2$. The solid lines in (d, e) represent exponential fits: ($y = 0.9 \exp(-t/\tau_1) + 0.1 \exp(-t/\tau_2)$, $\tau_1 = 35\text{ns}$, $\tau_2 = 240\text{ns}$ fits the decay in vacuum; $y = 0.95 \exp(-t/\tau_1) + 0.05 \exp(-t/\tau_2)$, $\tau_1 = 26\text{ns}$, $\tau_2 = 200\text{ns}$ fits the decay in low humidity and $y = \exp(-t/\tau)$, $\tau = 22\text{ns}$ fits the decay in high humidity. (f) Comparison of the Raman spectra at point B, under dry N_2 versus in a high humidity environment.

We hypothesize that the strained surface region grows and extends deeper into the crystal upon moisture exposure. Note that this phenomenon is partially reversible as shown by the recovery of the PL decay dynamics after storing the sample back in vacuum (Figure S4). To validate our hypothesis that exposure to the environment leads to a local distortion at the crystal surface we measured the micro-Raman spectra at the edge of the crystal in the presence of ambient humidity (Figure 2f). In particular, the peak at 109cm^{-1} shifts in energy and increases in intensity giving evidence for local distortion.^{11, 17} Additionally, the mode of the MA cation at 250cm^{-1} red shifts. This behaviour can be due to the effect of hydrogen bonding interactions between water molecules and the organic cations particularly relevant at the crystal edge. The centre of the crystal face, indeed, is less affected by interaction with humidity (see Figure S5 in the SI).

We remark here that the widening of the band gap observed upon moisture exposure along with structural distortion happening at the crystal edges are distinct from the optical and structural features related to perovskite conversion into its hydrated phases.^{21, 23, 26} Hydrated forms of MAPbI_3 , such as the $(\text{CH}_3\text{NH}_3)_4\text{PbI}_6 \cdot 2\text{H}_2\text{O}$ compound consisting of isolated PbI_6^{4-} octahedra,^{21, 23, 26, 29} are indeed pale yellow in colour, exhibit a bandgap of over 3 eV and a zero-dimensional structure.^{21, 23, 26} We therefore believe that what we observe is likely an initial step of structural reorganization towards conversion to a hydrated phase.

As evidenced by ab-initio molecular dynamics simulations,³⁰ water molecules can permeate across the perovskite structure to form a partly hydrated phase. Based on this preliminary observation, we further computationally simulated the possible phases obtained by the stepwise perovskite hydration. To investigate how water and oxygen molecules can interact with the hybrid perovskite we calculated the formation energies for $4\text{MAPbI}_3 \cdot n\text{H}_2\text{O}$ and $4\text{MAPbI}_3 \cdot \text{O}_2$ (Figure 3a and b, respectively), by scalar-relativistic Perdew-Burke-Ernzerhof (PBE) calculations employing van der Waals corrections. Starting from a tetragonal unit cell, consisting of four MAPbI_3 units, we sequentially add either one oxygen or up to four water molecules. The calculated relaxed atomic positions for $4\text{MAPbI}_3 \cdot \text{H}_2\text{O}$ and $4\text{MAPbI}_3 \cdot \text{O}_2$ are shown in Figure 3. Both structures exhibit an increase in the cell volume of $\sim 11\text{-}12 \text{ \AA}^3$ with respect to MAPbI_3 . While incorporation of one water molecule preserves the original tetragonal cell, with $a \approx b < c$ cell parameters, O_2 interaction with MAPbI_3 produces a sizable elongation/contraction of the a/b cell parameters ($a = 8.61$, $b = 8.81$, $c = 12.82$), respectively. Interestingly, as shown in Table S1 in the SI, the formation energy of $4\text{MAPbI}_3 \cdot 1\text{H}_2\text{O}$ is negative, (-0.45eV) indicating spontaneous water incorporation into the perovskite lattice. On the other hand, incorporation of molecular oxygen is unfavourable, with a positive ΔE_{form} of 0.17eV .

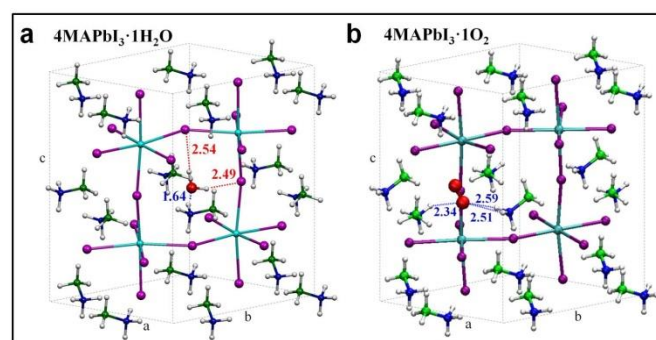


Figure 3. Optimized geometry structures for $4\text{MAPbI}_3 \cdot 1\text{H}_2\text{O}$ (a) and $4\text{MAPbI}_3 \cdot 1\text{O}_2$ (b). Pb= light blue, I=violet, green= carbon, blue=nitrogen, red=oxygen, white=hydrogen.

The driving force for water incorporation into the perovskite lattice is primarily the formation of hydrogen bonds between the water molecules and lattice iodides, as well as the tight hydrogen bonding interaction between one of the MA cations

and the water oxygen, as signalled by a ~ 1.6 Å separation distance between oxygen and one hydrogen atom of the MA cation (Figure 3a). Notably, O₂ interacts only through weaker hydrogen bonds with two vicinal MA cations, reflecting its lower tendency to be intercalated into the perovskite lattice. Water as well as oxygen (although less likely) incorporation into MAPbI₃ increases the band gap by 50 and 90 meV, respectively, estimated here at the scalar-relativistic level of theory used for geometry optimizations (see Table S1 for further details). While this level of theory is only able to accurately calculate the absolute bandgap values of lead halide perovskites due to a fortuitous cancellation of spin-orbit coupling effects,¹² the calculated variations in bandgap are still valid. Subsequent incorporation of water molecules into MAPbI₃ was also investigated up to a 4:4 stoichiometries (see Table S1 and Figure S6). The results show that incorporation of a second water molecule has an essentially additive effect on the perovskite properties, with a slight additional volume and bandgap increase as a result of lattice distortion. However, adding four water molecules destabilizes the perovskite lattice, resulting in a large band gap increase. This is consistent with reports of a large band gap hydrated MAPbI₃ phase with a non-perovskite structure.^{21,23,26,29} These findings support our experimental observations: the crystal edge surface, with a certain degree of distortion with respect to the bulk structure, is prone to water intercalation, resulting in a widening of the bandgap.

Experimental

MAPbI₃ Single Crystal Synthesis: All reagents were purchased from commercial vendors and used as received. Solid PbI₂ (0.20 g, 0.43 mmol) and methylammonium iodide (0.069 g, 0.43 mmol) were added to 3 mL of acetonitrile. Hydroiodic acid (200 μL, 57 wt. %, stabilized with 1.5 % hypophosphorous acid) was added to the acetonitrile mixture, which was then sonicated for 5 minutes to ensure complete dissolution of the precursors. Dark, highly reflective block crystals were obtained by allowing diffusion of diethyl ether into this solution over a period of 2 days. The crystals were washed three times with diethyl ether and then dried under reduced pressure. Single crystals were stored under nitrogen and then cleaved along the (110) plane before optical measurements.

Scanning Electron Microscopy (SEM): The sample was placed on conductive carbon tape. SEM observation was carried out using a high vacuum tungsten filament commercial Jeol 6010-LV, scanning electron microscope operating at 20 kV.

Macro-Photoluminescence: Time-resolved fluorescence measurements used for registering spectra and dynamics in Figure 2 were performed using a femtosecond laser source and a streak camera detection system (Hamamatsu C5680). For details on the experimental set-up see Refs. 3 and 19. The measurements were generally carried out in vacuum and the environmental conditions are explicitly stated in the manuscript when other conditions were used.

Micro-Raman and Micro-PL Spectroscopy: Our micro-Raman/PL system, used for measurements presented in Figure

1 b-d and Figure 2f, is based on an optical microscope (Renishaw microscope, see Ref. 11 for further details on the experimental apparatus). Samples are excited with a 532 nm laser diode. For the Raman measurement the spectra were registered in the 60-500 cm⁻¹ range. The final data was averaged over five hundreds acquisitions in order to improve the signal to noise ratio. The micro-PL has been registered simultaneously on the same micrometer-large spot of the sample in back reflection geometry in the range between 700 and 850 nm. To prevent sample degradation or thermal effects the laser power intensity is kept below 100 μW.

Computational Details: All calculations were carried out with the Quantum Espresso package along with the GGA-PBE functional. Electron-ion interactions were described by scalar relativistic ultrasoft pseudopotentials with electrons from O, N and C 2s, 2p; H 1s; I 5s, 5p; Pb 6s, 6p, 5d shells explicitly included in the calculations. Variable cell geometry optimizations were carried out including dispersion correction, as in Ref. 29. The formation energy of 4MAPbI₃•nH₂O has been evaluated as follows: $\Delta E_{\text{form}} = E(4\text{MAPbI}_3 \cdot n\text{H}_2\text{O}) - E(4\text{MAPbI}_3) - n \times E(\text{H}_2\text{O})$, where $E(4\text{MAPbI}_3 \cdot n\text{H}_2\text{O})$ is the energy of n-hydrated perovskite, $E(4\text{MAPbI}_3)$ is the energy of the anhydrous perovskite and $E(\text{H}_2\text{O})$ is the energy of the isolated water molecule. The same approach has been used to evaluate the formation energy of 4MAPbI₃•10O₂.

Conclusions

In conclusion, we demonstrate that the optical properties and band gap of MAPbI₃ single crystals are spatially inhomogeneous, particularly at their edge surfaces. The edge surface exhibits a larger band gap and shorter carrier recombination dynamics with respect to the centre. We demonstrate that the origin of this variation is structural in nature, resulting from lattice strain which may be attributed to surface reconstruction at the crystal edges. The degree of strain at the crystal edges can be modulated by exposure to moisture and possibly oxygen to a lesser extent. The sensitivity of the perovskite single crystal optical properties to environmental conditions and the balance between surface and edge effects can explain the discrepancies in optical spectra reported so far in the literature.⁵⁻⁹ The crystal edge surface further acts as an open gate for intercalation of water molecules, occurring spontaneously due to hydrogen bonding interactions with the perovskite lattice. This extends the depth of the surface region further into the bulk of the semiconductor, perhaps resulting in increased carrier trapping in optoelectronic devices. Regarding the moisture-induced degradation of perovskite optoelectronic devices, partial water intercalation into the perovskite structure is likely a necessary first step before structural conversion into a hydrate phase can occur. The observed blue-shift in the PL of perovskite crystals upon humidity exposure may provide an early warning signal before irreversible degradation occurs. Considering the tremendous interest in the application of such materials in optoelectronic devices, where the “interface is the device” (cit. Nobel laureate Herbert Kroemer) this work puts forward

important information on the local properties of active interfaces and grain boundaries in polycrystalline perovskite films.

Acknowledgements

The authors thank Dr. F. Tassone, Dr. James Ball and Dr. Ilaria Bargigia for valuable discussion and Giovanni De Vecchi and Marina Gandini for the SEM image. The research leading to these results has received funding from the European Union Seventh Framework Program [FP7/2007-2013] under grant agreement n° 604032 of the MESO project. E. T. H. and E.R.D. were supported through the Global Climate and Energy Project (GCEP). Single-crystal X-ray precession images were obtained at beamline 11.3.1 at the Advanced Light Source (ALS). The ALS is supported by the Director, Office of Science, Office of Basic Energy Sciences, of the U.S. Department of Energy under contract no. DE-AC02-05CH11231.

Notes and references

- H. Zhou, Q. Chen, G. Li, S. Luo, T.-b. Song, H.-s. Duan, Z. Hong, J. You, Y. Liu, Y. Yang, *Science* 2014, **345**, 542.
- M. Grätzel, *Nat. Mater.* 2014, **13**, 838.
- M. De Bastiani, V. D'Innocenzo, S. D. Stranks, H. J. Snaith, A. Petrozza, *APL Mater.* 2014, **2**, 081509.
- J.-H. Im, I.-H. Jang, N. Pellet, M. Grätzel, N.-G. Park, *Nat. Nanotechnol.* 2014, **9**, 927.
- H. Yu, F. Wang, F. Xie, W. Li, J. Chen, N. Zhao, *Adv. Funct. Mater.* 2014, **24**, 7102.
- D. Shi, V. Adinolfi, R. Comin, M. Yuan, E. Alarousu, A. Buin, Y. Chen, S. Hoogland, A. Rothenberger, K. Katsiev, Y. Losovyj, X. Zhang, P. A. Dowben, O. F. Mohammed, E. H. Sargent, O. M. Bakr, *Science* 2015, **347**, 519.
- Q. Dong, Y. Fang, Y. Shao, P. Mulligan, J. Qiu, L. Cao, J. Huang, *Science* 2015, **347**, 967.
- W. Nie, H. Tsai, R. Asadpour, J. C. Blancon, A. J. Neukirch, G. Gupta, J. J. Crochet, M. Chhowalla, S. Tretiak, M. A. Alam, H.-L. Wang, A. D. Mohite, *Science* 2015, **347**, 522.
- H. H. Fang, R. Raissa, M. Abdu-Aguye, S. Adjokatse, G. R. Blake, J. Even, M. A. Loi, *Adv. Funct. Mater.* 2015, **25**, 2378.
- S. De Wolf, J. Holovsky, S.-J. Moon, F. Löper, B. Niesen, M. Ledinsky, F.-J. Haug, J.-H. Yum, C. Ballif, *J. Phys. Chem. Lett.* 2014, **5**, 1035.
- G. Grancini, S. Marras, M. Prato, C. Giannini, C. Quarti, F. De Angelis, M. De Bastiani, G. E. Eperon, H. J. Snaith, L. Manna, A. Petrozza, *J. Phys. Chem. Lett.* 2014, **5**, 3836.
- E. Mosconi, A. Amat, Md. K. Nazeeruddin, M. Grätzel, F. De Angelis, *J. Phys. Chem. C* 2013, **117**, 13902.
- J. J. Choi, X. Yang, Z. M. Norman, S. J. L. Billinge, J. S. Owen, *Nano Lett.* 2014, **14**, 127.
- M. R. Filip, G. E. Eperon, H. J. Snaith, F. Giustino, *Nature Communications* 2014, **5**, 5757.
- A. Amat, E. Mosconi, E. Ronca, C. Quarti, P. Umari, Md. K. Nazeeruddin, M. Grätzel, F. De Angelis, *Nano Lett.* 2014, **14**, 3608.
- E. Mosconi, C. Quarti, T. Ivanovska, G. Ruani, F. De Angelis, *Phys. Chem. Chem. Phys.* 2014, **16**, 16137.
- C. Quarti, G. Grancini, E. Mosconi, P. Bruno, J. M. Ball, M. M. Lee, H. J. Snaith, A. Petrozza, F. De Angelis, *J. Phys. Chem. Lett.* 2014, **5**, 279.
- E. T. Hoke, D. J. Slotcavage, E. R. Dohner, A. R. Bowring, H. I. Karunadasa, M. D. McGehee, *Chem. Sci.* 2015, **6**, 613.
- V. D'Innocenzo, A. R. Srimath Kandada, M. De Bastiani, M. Gandini, A. Petrozza, *J. Am. Chem. Soc.* 2014, **136**, 17730.
- C. Motta, F. El-Mellouhi, S. Kais, N. Tabet, F. Alharbi, S. Sanvito, *Nat. Commun.* 2015, **6**, 7026.
- A. Leguy, Y. Hu, M. Campoy-Quiles, M. I. Alonso, O. J. Weber, P. Azarhoosh, M. Van Schilfgaarde, M. T. Weller, T. Bein, J. Nelson, P. Docampo, P. R. F. Barnes *Chem. Mater.* 2015, **27**, 3397.
- J. You, Y. (M.) Yang, Z. Hong, T.-b Song, L. Meng, Y. Liu, C. Jiang, H. Zhou, W.-H. Chang, G. Li, Y. Yang, *Appl. Phys. Lett.* 2014, **105**, 183902.
- J. A. Christians, P. A. Miranda Herrera, P. V. Kamat, *J. Am. Chem. Soc.* 2015, **137**, 1530.
- X. Dong, X. Fang, M. Lv, B. Lin, S. Zhang, J. Ding, N. Yuan, *J. Mater. Chem. A* 2015, **3**, 5360.
- K. K. Bass, R. E. McAnally, S. Zhou, P. I. Djurovich, M. E. Thompson, B. C. Melot, *Chem. Comm.* 2014, **50**, 15819.
- J. Yang, B. D. Siempelkamp, D. Liu, T. L. Kelly, *ACS Nano* 2015, **9**, 1955.
- S. Pathak, A. Sepe, A. Sadhanala, F. Deschler, A. Haghighirad, N. Sakai, K. C. Goedel, S. D. Stranks, N. Noel, M. Price, S. Hüttner, N. A. Hawkins, R. H. Friend, U. Steiner, H. J. Snaith, *ACS Nano* 2015, **9**, 2311.
- N. Aristidou, I. Sanchez-Molina, T. Chotchuangchutchaval, M. Brown, L. Martinez, T. Rath, S. A. Haque, *Angew. Chem.* 2015, **127**, 8326.
- B. R. Vincent, K. N. Robertson, T. S. Cameron, O. Knop, *Can. J. Chem.*, 1987, **65**, 1042.
- E. Mosconi, J. M. Azpiroz, F. De Angelis, *Chem. Mater.* 2015, doi: 10.1021/acs.chemmater.5b01991